

# Acid–base behavior, electrochemical properties and DFT study of redox non-innocent phenol–imidazole ligands and their Cu complexes



Arfa Parween<sup>a</sup>, Tarun Kanti Mandal<sup>b</sup>, Régis Guillot<sup>c</sup>, Subhendu Naskar<sup>a,\*</sup>

<sup>a</sup> Department of Chemistry, Birla Institute of Technology, Mesra, Ranchi 835215, Jharkhand, India

<sup>b</sup> Department of Biotechnology, Haldia Institute of Technology, Hatiberia, Haldia 721 657, West Bengal, India

<sup>c</sup> Université Paris Sud, ICMMO-ECI, UMR CNRS 8182, Université Paris-Sud, 91405 Orsay, France

## ARTICLE INFO

### Article history:

Received 13 April 2015

Accepted 10 June 2015

Available online 17 June 2015

### Keywords:

Imidazole–phenol ligands

$pK_a$

Electronic spectra

Cyclic voltammetry

DFT calculation

## ABSTRACT

Three Cu complexes (**1**, **2**, **3**) with N, O donor ligands having imidazole–phenol moieties 2-(4,5-diphenyl-1H-imidazol-2-yl)phenol (**L<sup>1</sup>H**), 4-bromo 2-(4,5-diphenyl-1H-imidazol-2-yl)phenol (**L<sup>2</sup>H**) and 1-(4,5-diphenyl-1H-imidazol-2-yl)naphthalene-2-ol (**L<sup>3</sup>H**) have been synthesized and characterized by spectroscopic techniques. Molecular structure of one Cu complex (**2**) has been determined by X-ray crystallography. **2-DMF** crystallises in monoclinic  $P2_1/c$  space group with an exactly intermediate geometry between tetrahedral and square planar ( $\tau_4 = 0.5319$ ). The  $pK_a$  values of the ligands were determined by UV–Vis spectrophotometric titration. The imidazole–phenol ligand exhibit a high sensitivity towards the pH of the solution.  $pK_a$  of the imidazolium cation is  $\sim 4.1$ , whereas  $pK_a$  for the phenolic deprotonation is in the range 10–10.7. Electronic spectra of the complexes consist of a phenoxide to  $Cu^{II}$  LMCT in the region (490–500 nm) and a d–d transition in the range (620–716 nm). All the ligands and the complexes exhibit one ligand based oxidation: phenol/phenoxy radical or phenolate/phenoxy radical. pH dependent electrochemical study shows the oxidation process is highly pH sensitive. Potential for this oxidation is close to that observed in Galactose oxidase.

© 2015 Published by Elsevier Ltd.

## 1. Introduction

Tyrosine is a very important component in nature involved in a number of enzyme catalysis. Tyrosyl radical is the species in all these processes [1]. This radical is observed in three different forms: (i) coordinated to  $Cu^{II}$  (Galactose oxidase or Glyoxal oxidase) [2], (ii) free (IRNR–iron dependent ribonucleotide reductase) [3] and (iii) hydrogen bonded (Photosystem II) [4]. All these reactions take place through a fundamental step: oxidation of tyrosine to tyrosyl radical. For a better understanding of enzymatic mechanism oxidation of phenol, particularly electrochemically has attracted the researchers a lot. Electrochemical oxidation of phenol is assisted by transfer of the phenolic proton to a base. The later may be intramolecular or intermolecular. In presence of bases the PCET (Proton coupled electron transfer) processes in phenols have been thoroughly studied by Savéant et al. [5–7]. As intramolecular base amines [8–10], pyrazoles [11,12], imidazoles [13–16] or benzimidazoles [17] have been used at the ortho position of phenolic–OH. The phenoxy radical also achieves an

enhanced stability when coordinated to metals, as seen from the low oxidation potential for the phenolate/phenoxy couple in the complex. Benisvy et al. reported a number of complexes of pyrazole/imidazole–phenolate with Cu, Co or Zn [11–16]. Kochem et al. reported [18] a system highlighting the effect of steric strain in the Cu complex on the phenolate/phenoxy oxidation process.

Electrochemical oxidation of phenol is pH dependent, the dependency increases in presence of a base [5–7]. But the electrochemical behavior of the phenol with an adjacent imidazole moiety which can resemble the natural system, e.g., PSII, galactose oxidase is less explored. In this context here in we report a phenol–imidazole system and its Cu complexes. The electrochemical behaviors of the ligands and the complexes have been studied by means of cyclic voltammetry. The ligand system used in the present study contains three different sites for deprotonation: protonated imidazole–N, phenolic–OH and imidazole proton.  $pK_a$  of the first two dissociation were measured for our system. The 3rd dissociation step was not achievable due to the precipitation at pH >13. The  $pK_a$  values of the ligands and the complexes were determined by UV–Vis spectrophotometric and electrochemical titration. In the present system we noticed the sharp decrease in  $pK_a$  of the imidazolium cation. The enhanced acidity of the imidazolium ion is proposed to the favorable formation of the highly

\* Corresponding author. Tel.: +91 0651 2275631x4476; fax: +91 0651 2276052.  
E-mail address: [subnaskar@yahoo.co.in](mailto:subnaskar@yahoo.co.in) (S. Naskar).

stabilised conjugate base through intramolecular hydrogen bonding between phenolic-OH and imidazole-N.

## 2. Experimental

### 2.1. Materials

All reagents and chemicals were purchased from commercial sources like E. Merck, Fluka and Aldrich and used without further purification. HPLC grade MeCN, DMF, DMSO and DCM were used for spectroscopic and electrochemical studies. All solvents were A.R. grade and used as received for synthetic work. Tetra ethyl ammonium perchlorate (TEAP), used for the electrochemical studies was prepared according to the literature [19].

### 2.2. Physical measurements

Elemental analyses were performed on an Elementar Vario EL III C, H, N, S & O analyzer. Infrared spectra were recorded as KBr pellets on a Shimadzu IR-Prestige21 spectrometer. Electronic spectra were recorded on a Perkin Elmer Lambda 750 Spectrophotometer. To determine the  $pK_a$  value of the ligands and complexes, a series of DMF–aqueous buffer (Robinson–Britton) solution (1:1) of  $7.5 \times 10^{-5}$  M of analyte having different pH (range 3–13) were prepared for spectrophotometric titration. The pH values were measured in a Thermo Scientific Orion 4 star pH Benchtop.

Electrochemical measurements of all the ligands and complexes were recorded in the presence of different pH in DMF:H<sub>2</sub>O (8:2) containing 0.1 M TEAP as supporting electrolyte, using a CHI6003E potentiostat, glassy carbon working electrode, Pt wire as a counter electrode and Ag/AgCl non aqueous reference electrode. The ferrocene/ferrocenium couple was observed at  $E^0$  ( $\Delta E_p$ ) = 0.4 V (100 mV) under these experimental conditions.

<sup>1</sup>H NMR spectra were recorded on a Bruker AVANCE DPX 500 MHz spectrometer using, Si(CH<sub>3</sub>)<sub>4</sub> as internal standard. ESI-MS spectra of the samples were recorded on JEOL JMS 600 instrument.

### 2.3. Synthesis of the ligands

2-(4,5-Diphenyl-1H-imidazol-2-yl)phenol (**L<sup>1</sup>H**): 2-(4,5-diphenyl-1H-imidazol-2-yl)phenol was synthesized by the reaction of Benzil (1.05 g, 5 mmol), Salicylaldehyde (0.61 g, 5 mmol) and Ammonium Acetate (7.70 g, 100 mmol) in 5 ml acetic acid. The reaction mixture was refluxed for 4 h. A white color precipitate (**L<sup>1</sup>H**) obtained, it was filtered in vacuum, washed with distilled water (4 × 5 ml) and dried at room temperature.

Yield: (0.96 g) 62%, NMR (<sup>1</sup>H, 500 MHz, CDCl<sub>3</sub>):  $\delta$  12.72 (s, 1H, N-H), 9.37 (s, 1H, O-H), 6.90–7.47 (m, 14H, ArH); Elemental Anal. Calc. for C<sub>21</sub>H<sub>16</sub>N<sub>2</sub>O: C, 80.75; H, 5.16; N, 8.97. Found: C, 79.60; H, 5.73; N, 8.13%. IR (KBr, cm<sup>-1</sup>):  $\nu$  3201, 3057, 1593, 1492, 1381, 1261, 763, 692. MS:  $m/z$  313 {M+}.

4-Bromo 2-(4,5-diphenyl-1H-imidazol-2-yl)phenol (**L<sup>2</sup>H**): 4-Bromo 2-(4,5-diphenyl-1H-imidazol-2-yl)phenol was synthesized by the reaction of Benzil (1.05 g, 5 mmol), 5-Br-Salicylaldehyde (1.00 g, 5 mmol) and Ammonium Acetate (7.70 g, 100 mmol) in 5 ml acetic acid. A white colored precipitate (**L<sup>2</sup>H**) was prepared by similar procedure as for, ligand (**L<sup>1</sup>H**).

Yield: (1.38 g) 71%, NMR (<sup>1</sup>H, 500 MHz, CDCl<sub>3</sub>):  $\delta$  6.949 (d, 1H, ArH), 7.260–7.770 (m, 11H, ArH), 7.78 (m, 1H, ArH); Elemental Anal. Calc. for C<sub>21</sub>H<sub>15</sub>BrN<sub>2</sub>O: C, 64.46; H, 3.86; N, 7.16. Found: C, 64.06; H, 3.22; N, 6.91%. IR (KBr, cm<sup>-1</sup>):  $\nu$  3195, 3057, 1577, 1487, 1371, 1251, 810, 769, 696. MS:  $m/z$  391 {M+}.

1-(4,5-Diphenyl-1H-imidazol-2-yl)naphthalene-2-ol (**L<sup>3</sup>H**): 1-(4,5-diphenyl-1H-imidazol-2-yl)naphthalene-2-ol was synthesized by the reaction of Benzil (1.05 g, 5 mmol), 2-Hydroxy-1-naphthaldehyde (0.86 g, 5 mmol) and Ammonium Acetate (7.70 g, 100 mmol) in 5 ml acetic acid. A light yellow colored precipitate (**L<sup>3</sup>H**) was prepared by similar procedure as for, ligand (**L<sup>1</sup>H**).

Yield: (1.3 g) 72%, NMR (<sup>1</sup>H, 500 MHz, CDCl<sub>3</sub>):  $\delta$  7.26–7.63 (m, 13H, ArH), 7.79 (d, 1H, ArH), 7.86 (d, 1H, ArH), 8.21 (d, 1H, ArH); Elemental Anal. Calc. for C<sub>25</sub>H<sub>18</sub>N<sub>2</sub>O: C, 82.85; H, 5.01; N, 7.73. Found: C, 82.51; H, 4.98; N, 7.68%. IR (KBr, cm<sup>-1</sup>):  $\nu$  3246, 3053, 2663, 1707, 1589, 1479, 1334, 1249, 758, 699. MS:  $m/z$  363 {M+}.

### 2.4. Synthesis of the complexes

#### General procedure for the synthesis of [Cu(L)<sub>2</sub>] compounds

The 2 equivalent of prepared ligand was completely dissolved in methanol. 2 equivalent of Et<sub>3</sub>N were added followed by 1 equivalent of Cu(ClO<sub>4</sub>)<sub>2</sub>·6H<sub>2</sub>O. The reaction mixture was refluxed for 5 h and the product was isolated and purified according to the particular procedure described below.

[Cu(L<sup>1</sup>H)<sub>2</sub>] (**1**): Cu(ClO<sub>4</sub>)<sub>2</sub>·6H<sub>2</sub>O (185.2 mg, 0.5 mmol) in MeOH (10 ml) and L<sup>1</sup>H (312 mg, 1 mmol) in MeOH (15 ml) were reacted as described above. A brown precipitate of complex **1** was washed by methanol and ether, finally dried in vacuum. Yield: (205.8 mg) 60%; Elemental Anal. Calc. for Cu-C<sub>42</sub>H<sub>32</sub>N<sub>4</sub>O<sub>2</sub>: C, 73.29; H, 4.69; N, 8.14. Found: C, 73.28; H, 4.13; N, 7.42%. IR (KBr, cm<sup>-1</sup>):  $\nu$  3057, 1604, 1479, 1315, 1255, 769, 696. MS:  $m/z$  708 {M+Na}, 686 {M+}. UV-Vis (DMF):  $\lambda_{max}/nm$  ( $\epsilon/M^{-1} cm^{-1}$ ): 290 (49818), 320 (61678), 364sh (12545), 490 (643), 716 (310).

[Cu(L<sup>2</sup>H)<sub>2</sub>] (**2**): Cu(ClO<sub>4</sub>)<sub>2</sub>·6H<sub>2</sub>O (185.2 mg, 0.5 mmol) in MeOH (10 ml) and L<sup>2</sup>H (391 mg, 1 mmol) in MeOH (15 ml) were reacted as described above. A brown precipitate of complex **2** was washed by methanol and ether, finally dried in vacuum. Yield: (286.2 mg) 68%; single crystals, suitable for X-ray crystallography was obtained from DMF solution. Elemental Anal. Calc. for Cu-C<sub>42</sub>H<sub>30</sub>Br<sub>2</sub>N<sub>4</sub>O<sub>2</sub>: C, 59.62; H, 3.57; N, 6.62. Found: C, 59.31; H, 3.51; N, 6.14%. IR (KBr, cm<sup>-1</sup>):  $\nu$  3055, 2868, 1596, 1477, 1301, 1251, 815, 771, 696. MS:  $m/z$  843 {M+}. UV-Vis (DMF):  $\lambda_{max}/nm$  ( $\epsilon/M^{-1} cm^{-1}$ ): 296 (29773), 335 (24322), 344 (26785), 374sh (14588), 500 (752), 712 (378).

**Table 1**

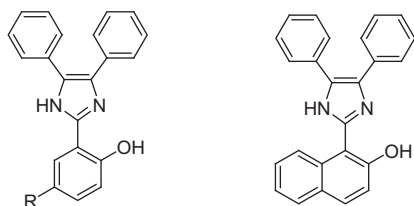
Crystal data and details of the structure determination for **2DMF**.

Empirical formula	C <sub>42</sub> H <sub>28</sub> Br <sub>2</sub> CuN <sub>4</sub> O <sub>2</sub> , C <sub>3</sub> H <sub>7</sub> NO
Formula weight	917.14
Crystal system	monoclinic
Crystal size (mm)	0.32 × 0.09 × 0.01
Space group	P2 <sub>1</sub> /c
<i>a</i> (Å)	18.8571(13)
<i>b</i> (Å)	15.9999(11)
<i>c</i> (Å)	13.3625(8)
$\alpha$ (°)	90
$\beta$ (°)	96.2360(10)
$\gamma$ (°)	90
Cell volume (Å <sup>3</sup> )	4007.8(5)
<i>Z</i>	4
<i>T</i> (K)	100(1)
<i>F</i> (000)	1852
$\mu$ (mm <sup>-1</sup> )	2.526
$\theta$ range (°)	1.09–30.54
Reflection collected	48695
Reflections unique	12079
<i>R</i> <sub>int</sub>	0.1425
GOF	0.976
Refl. obs. ( <i>I</i> > 2 $\sigma$ ( <i>I</i> ))	5103
Parameters	507
<i>wR</i> <sub>2</sub> (all data)	0.1456
<i>R</i> value ( <i>I</i> > 2 $\sigma$ ( <i>I</i> ))	0.0239
Largest diff. peak and hole (e <sup>-</sup> Å <sup>-3</sup> )	-1.183; 1.237

$[Cu(L^3H)_2]$  (**3**):  $Cu(ClO_4)_2 \cdot 6H_2O$  (185.2 mg, 0.5 mmol) in MeOH (10 ml) and  $L^3H$  (363 mg, 1 mmol) in MeOH (15 ml) were reacted as described above. A Gray color precipitate of complex **3** was washed by methanol and ether, finally dried in vacuum. Yield: (255.4 mg) 65%; Elemental Anal. Calc. for  $Cu-C_{50}H_{36}N_4O_2$ : C, 76.17; H, 4.60; N, 7.11. Found: C, 76.09; H, 4.03; N, 7.03%. IR (KBr,  $cm^{-1}$ ):  $\nu$  3053, 2816, 1602, 1539, 1463, 1371, 758, 696. MS:  $m/z$  786  $\{M^+\}$ . UV–Vis (DMF):  $\lambda_{max}/nm$  ( $\epsilon/M^{-1} cm^{-1}$ ): 304 (53930), 356 (33400), 492sh (521), 620 (352).

## 2.5. X-ray crystallography

X-ray diffraction data was collected by using a Kappa X8 APPEX II Bruker diffractometer with graphite-monochromated Mo  $K\alpha$  radiation ( $\lambda = 0.71073 \text{ \AA}$ ). Crystals were mounted on a CryoLoop (Hampton Research) with Paratone-N (Hampton Research) as cryoprotectant and then flashfrozen in a nitrogen-gas stream at 100 K. The temperature of the crystal was maintained at the selected value (100 K and 200 K) by means of a 700 series Cryostream



Ligand: R = H ( $L^1H$ ), R = Br ( $L^2H$ ) ( $L^3H$ )

Complex:  $[Cu(L^1H)_2]$  (**1**),  $[Cu(L^2H)_2]$  (**2**)  $[Cu(L^3H)_2]$  (**3**)

**Fig. 1.** Chemical formula of the ligands and complexes.

cooling device to within an accuracy of  $\pm 1$  K. The data were corrected for Lorentz polarization, and absorption effects. The structures were solved by direct methods using SHELXS-97 [20] and refined against  $F^2$  by full-matrix least-squares techniques using SHELXL-97 [21] with anisotropic displacement parameters for all non-hydrogen atoms. Hydrogen atoms were located on a difference Fourier map and introduced into the calculations as a riding model with isotropic thermal parameters. All calculations were performed by using the Crystal Structure crystallographic software package WINGX [22]. The crystal data collection and refinement parameters are given in Table 1.

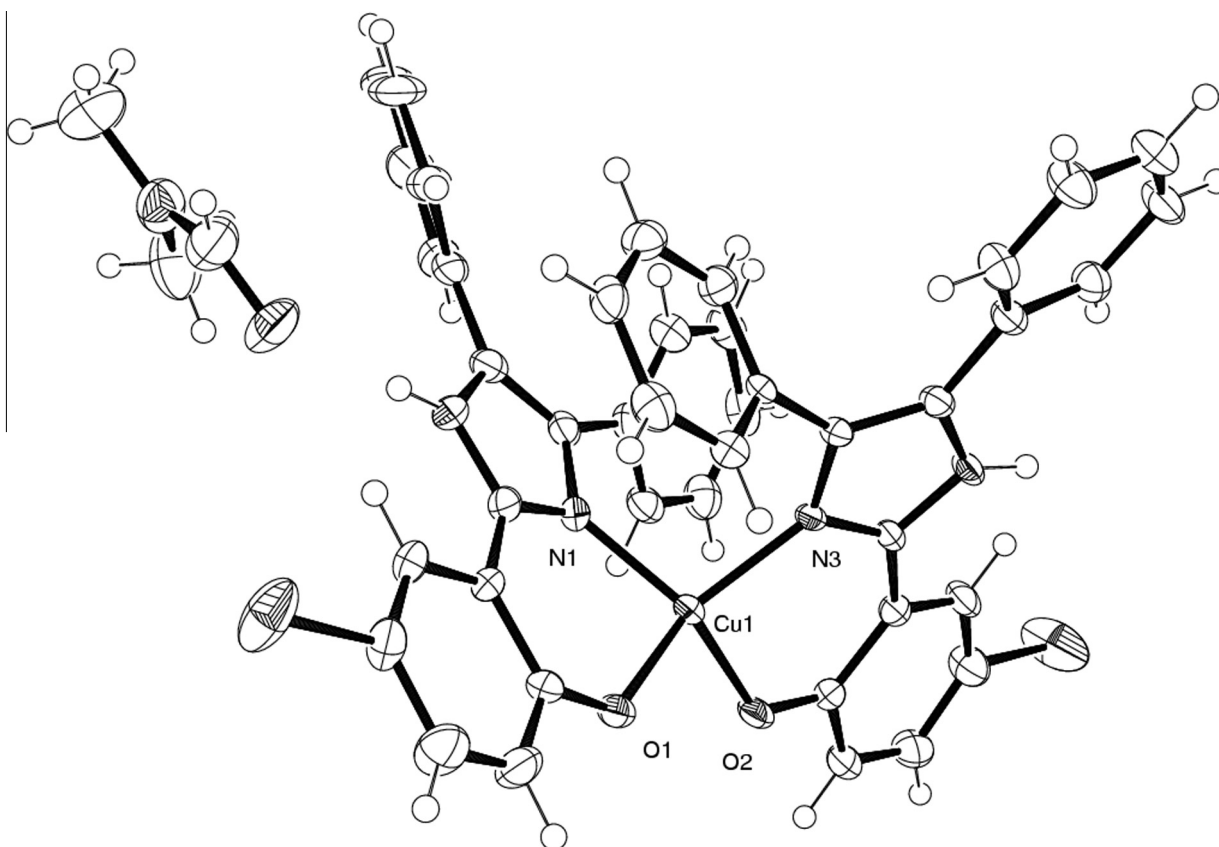
## 2.6. Computational detail

All the calculations were performed using density functional theory (DFT) implemented in GAUSSIAN09 [23]. All the geometrical isomer of the complex were fully optimized using B3LYP hybrid functional and 6-31g(d) basis set for hydrogen, carbon, oxygen, nitrogen and bromine and LANL2DZ basis set for copper. The absorption spectra were simulated using Time Dependent Density Functional Theory (TD-DFT). All the computational study was carried out in DMF solvent using Polarizable Continuum Model (PCM) implemented in Gaussian 09. The multiplicity of the complex is doublet. Therefore the transition occurs within Alpha MO or Beta MO, indicated by A or B in bracket, respectively.

## 3. Results and discussion

### 3.1. Synthesis

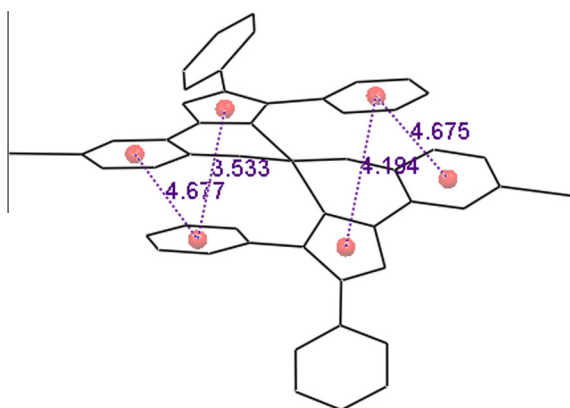
The ligands reported here (Fig 1) were synthesised following literature [13,14] by 1:1 condensation of salicylaldehyde/substituted



**Fig. 2.** ORTEP diagram of **2-DMF** with atom numbering scheme at 50% ellipsoid probability.

**Table 2**  
Selected bond lengths (Å) and bond angles (°) for complex **2-DMF**.

Bond lengths	
N1Cu1	1.911(3)
N3Cu1	1.964(3)
O1Cu1	1.923(3)
O2Cu1	1.890(3)
Bond angles	
O2Cu1N1	146.78(15)
O2Cu1O1	93.27(12)
N1Cu1O1	91.91(13)
O2Cu1N3	94.45(12)
N1Cu1N3	102.82(13)
O1Cu1N3	139.11(14)

**Fig. 3.**  $\pi$ - $\pi$  staking interactions between the phenyl ring and phenol-imidazole ring.**Table 3**  
List of hydrogen bonds.

Donor-H...acceptor	D-H (Å)	H...A (Å)	D...A (Å)	$\angle$ D-H...A (°)
N(2)-H(2A)...O(3)	0.86	1.95	2.806(5)	174
N(4)-H(4)...O(1) <sup>i</sup>	0.86	2.05	2.868(4)	159
C(5)-H(5)...O(3) <sup>i</sup>	0.93	2.52	3.413(6)	160
C(38)-H(38)...O(2)	0.93	2.32	3.233(6)	166

$$i = x, 1/2 - y, -1/2 + z.$$

salicylaldehyde and benzil in acetic acid medium in the presence of an excess of Ammonium acetate. Salicylaldehyde, 5-Br-salicylaldehyde and 2-hydroxy naphthaldehyde were used for the preparation of L<sup>1</sup>H, L<sup>2</sup>H and L<sup>3</sup>H, respectively. Cu(ClO<sub>4</sub>)<sub>2</sub>·6H<sub>2</sub>O reacted

with each of the ligand (1:2) in the presence of Et<sub>3</sub>N to form the neutral compound [Cu(L)<sub>2</sub>].

### 3.2. Description of the X-ray crystal structures

The Brown colored Single Crystal of **2-DMF** was obtained from evaporation of DMF solution of **2**. A molecular structure of **2-DMF** has been determined by single crystal X-ray diffraction (Fig. 2).

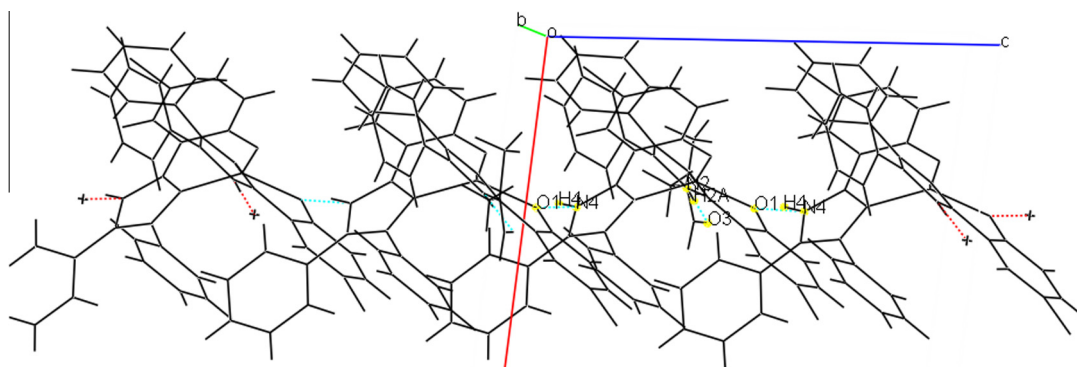
**2-DMF** crystallises in monoclinic *P2<sub>1</sub>/c* space group. Cu(II) is in a N<sub>2</sub>O<sub>2</sub> donor environment of the ligand. **2-DMF** adopts a distorted tetrahedral/square planer geometry, Cu(II) being coordinated by two imidazole-N (N1, N3) and two phenolic-O (O1, O2) atoms. The degree of distortion from either of the geometry is quite clear from the bond angles. Selected bond length and bond angles are given in Table 2. Three cis-angles (93.27(12), 91.91(13), 94.45(12)) are very close to the ideal value for square planar arrangement with significant deviation in the fourth one (102.82(13)). The trans angles (146.78(15), 139.11(14)) are very much different from the ideal square planar value of 180°. The bond lengths and angles are similar to the earlier reports [14]. Actually it is an intermediate structure of tetrahedral and square planar geometry. The degree of distortion can be calculated from four coordinate geometry index  $\tau_4$  [24].  $\tau_4$  is obtained from the relation.

$$\tau_4 = \frac{360^\circ - (\alpha + \beta)}{141^\circ}$$

where  $\alpha$  and  $\beta$  are the two largest angles.  $\tau_4 = 1$  and 0 for perfect tetrahedral and square planar geometry respectively. The present molecule has  $\tau_4 = 0.5319$ , indicating an intermediate geometry of tetrahedral and square planar being slightly closer to the former.

Surprisingly **2-DMF** adopts a cis geometry for the two phenol rings (O2-Cu1-O1 angle = 93.27° (12)), leaving the four phenyl rings attached at the 4 and 5 positions of the two imidazole from the two ligands at the same side of Cu. The steric demand for this arrangement might have been overcome by the presence of  $\pi$ - $\pi$  staking interactions of one phenyl group of one ligand with and the phenol and imidazole rings of the other ligand (Fig. 3). Similar types of interactions have also been reported by Benisvy et al. [14].

Imidazole-N-H (H4) of one ligand and phenoxide-O (O1) of the other ligand of an asymmetric unit form intermolecular hydrogen bonds (Table 3). With respect to the Cu these H-bonds donor and acceptor are situated in opposite direction along crystallographic *c* axis (Fig. 4). Therefore the N4-H4...O1 bonds form a supramolecular chain along *c*-axis. The imidazole-H of the same ligand is attached to the solvent DMF through hydrogen bond N2-H2A...O3.

**Fig. 4.** Hydrogen bonded supramolecular chain along crystallographic *c* axis.

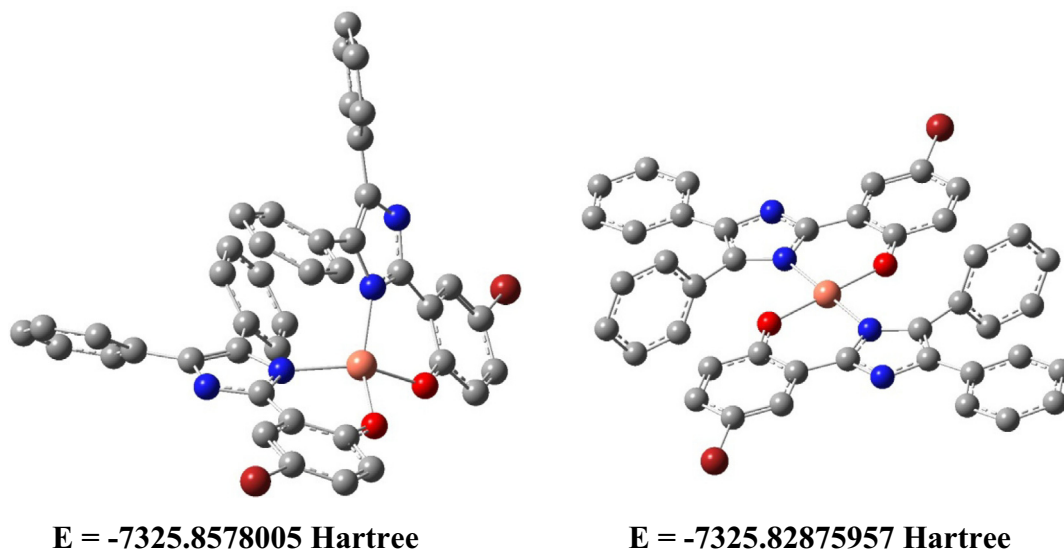


Fig. 5. Optimized structure for the tetrahedral and square planar geometry with energy for complex 2.

Table 4

Bond length and bond distances of the crystal geometry and optimized geometry for complex 2.

Geometry bond	Crystal geometry distance (Å)	Optimized geometry (tetrahedral)
N1 Cu1	1.911(3)	2.01
N3 Cu1	1.964(3)	2.01
O1 Cu1	1.923(3)	1.94
O2 Cu1	1.890(3)	1.94
O2 Cu1 N1	146.78(15)	150.18
O2 Cu1 O1	93.27(12)	89.84
N1 Cu1 O1	91.91(13)	90.47
O2 Cu1 N3	94.45(12)	90.46
N1 Cu1 N3	102.82(13)	103.6
O1 Cu1 N3	139.11(14)	150.15

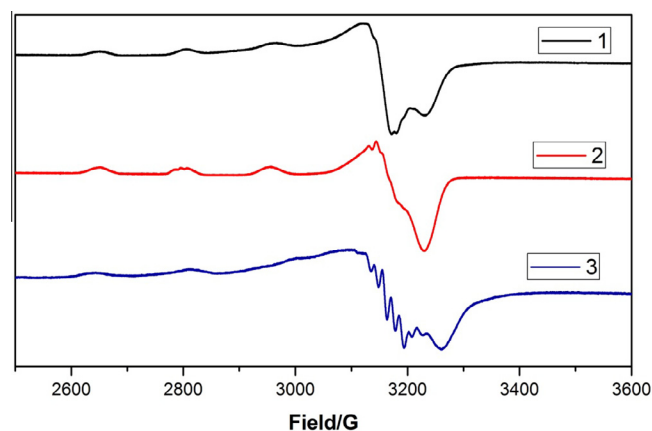


Fig. 7. X-band EPR spectra of 1, 2 and 3 in DMF recorded at 77 K.

Table 5

$g$  and  $A$  values in the EPR spectra for the complexes 1, 2 and 3.

Complex	$g_1$	$g_2$	$g_3$	$A\{^{63,65}\text{Cu}\}/\text{G}$	$a\{^{14}\text{N}\}/\text{G}$
1	2.25	2.05	2.01	155	8
2	2.26	2.05	2.06	153	–
3	2.23	2.06	1.99	178	15

O of the adjacent molecule. Collectively the crystal forms supramolecular structure by two hydrogen bonds, two short contacts and two set of  $\pi$ – $\pi$  stacking interactions.

Computational study using Density functional theory with B3LYP hybrid functional was performed to get the optimized structure of the ligand  $\text{L}^2\text{H}$  and the complex 2. Both square planar and tetrahedral structures were optimized (Fig. 5). The energy of both the structure is almost same, tetrahedral structure ( $E = -7325.8578005$  Hartree) being slightly more stable than the square planar ( $E = -7325.82875957$  Hartree). In practice four coordinate geometry index  $\tau_4$  obtained for the molecule is exactly at the intermediate of square planar and tetrahedral geometry. A comparison between the experimental and optimized structure for the coordination sphere is given in Table 4. The similarity in the crystal

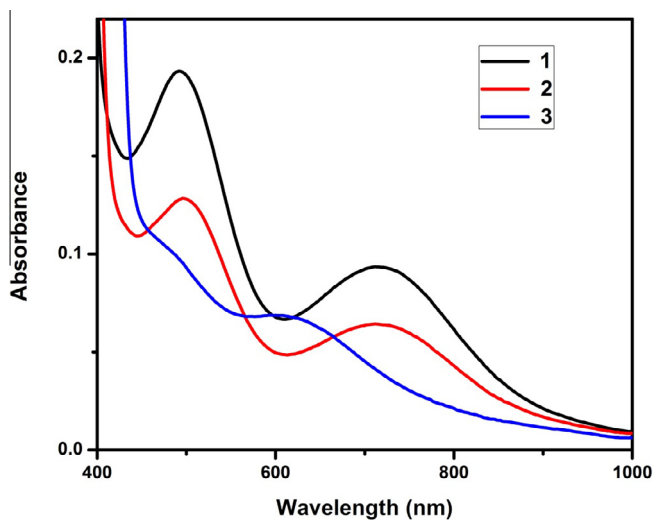


Fig. 6. Absorbance spectra of complexes (1, 2 and 3) in the visible region in DMF.

In addition two other short contacts also exist: C5–H5...O3 connects the phenol ring hydrogen with O atom of DMF molecule and C38–H38...O2 connects one phenyl ring with the phenoxide-

**Table 6**

Vertical excitations with band position, oscillator strength and character assignment.

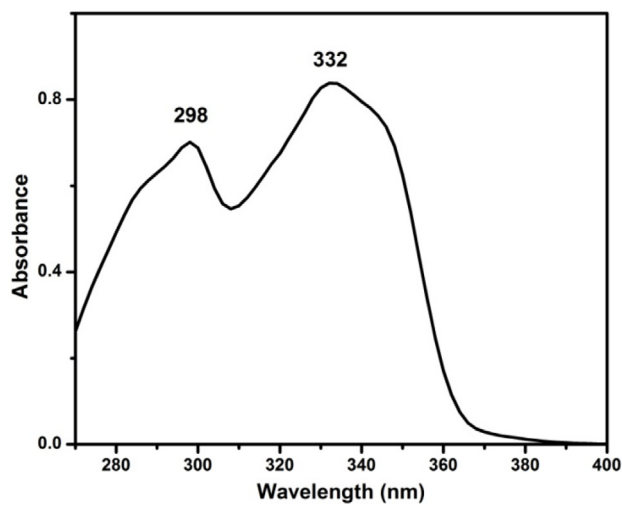
Comp/Lig	Experimental wave length (nm)	Wave length obtained from TD-DFT (nm)	Oscillator strength (f)	Contributing orbital (s)	Percent age (%)	Transition assignment
<b>2</b>	296	293	0.14	HOMO – 2(A) → LUMO(A)	36	Intra ligand
	335	335	0.38	HOMO – 1(A) → LUMO + 1(A)	48	Intra ligand
	344	350.75	0.16	HOMO(A) → LUMO + 1(A)	21	Intra ligand
	374	367	0.12	HOMO(A) → LUMO(A)	17	Intra ligand
	500	498.65	0.0003	HOMO – 3(B) → LUMO(B)	33	LMCT
		529.2	0.003	HOMO – 2(B) → LUMO(B)	29	LMCT
	712	665.86	0.05	HOMO – 24(B) → LUMO(B)	14	d–d(ligand assisted)
				HOMO – 7(B) → LUMO(B)	17	LMCT
<b>(L<sup>2</sup>H)</b>	298	308	0.3062	HOMO → LUMO + 1	98	Imidazole → Benzene
	332	335	0.6614	HOMO → LUMO	98	Imidazole → Phenol

geometry and the optimized structure indicates that the level of calculation is quite good for this type of molecule.

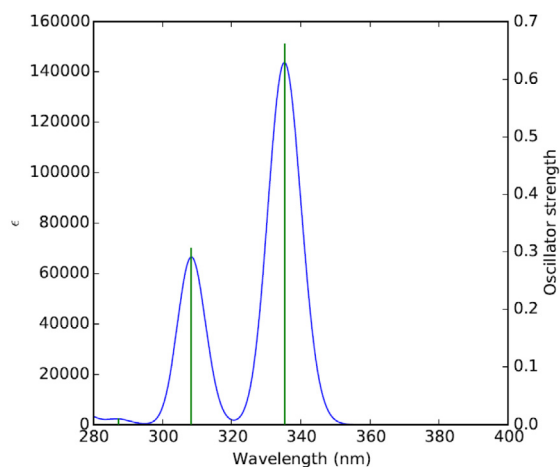
### 3.3. Electronic spectra

The UV–Vis absorption spectra of the ligands display two distinct peaks in the region 290–308 nm and 320–353 nm (Fig. S10).

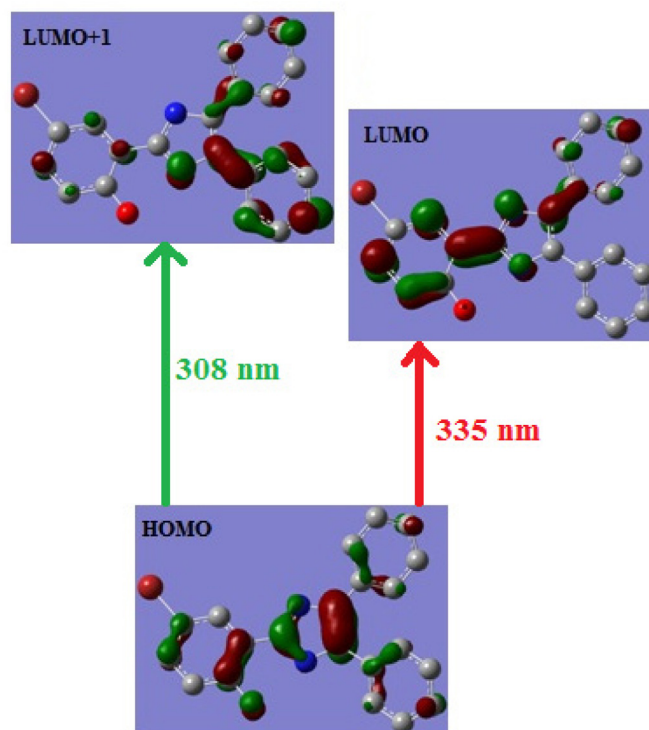
These UV region transitions are also observed in the corresponding Cu complexes and may be assigned as intraligand transition. The low energy UV transition for L<sup>3</sup>H ( $\lambda = 353$  nm) appears at quite longer wavelength than L<sup>1</sup>H ( $\lambda = 320$  nm) and L<sup>2</sup>H ( $\lambda = 332$  nm). TD-DFT calculation on one of the ligand L<sup>2</sup>H shows that this transition takes place from imidazole ring to phenol ring. This may also take place for L<sup>1</sup>H and L<sup>3</sup>H. Due to better delocalising capacity of



(a)



(b)



(c)

**Fig. 8.** (a) L<sup>2</sup>H-experimental spectra. (b) L<sup>2</sup>H-simulated spectra. (c) Electronic transition in L<sup>2</sup>H at 308 nm and 335 nm in DMF.

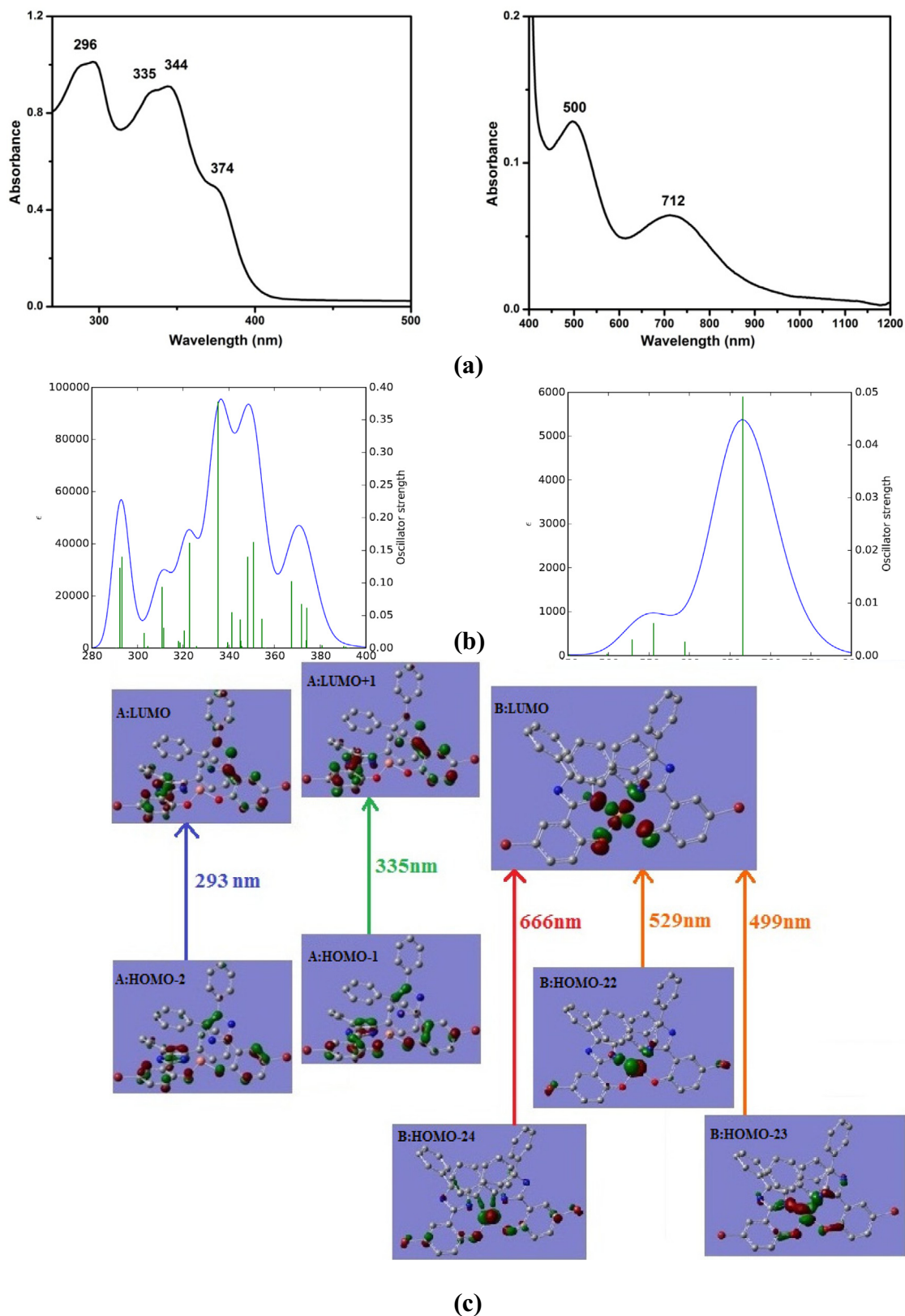


**Fig. 9.** (a) Complex 2-experimental spectra, (b) Complex 2-simulated spectra. (c) Electronic transition in complex 2 at 293 nm, 335 nm, 499 nm, 529 nm and 666 nm and in DMF medium.

the naphthyl ring ( $L^3H$ ) than phenol ring ( $L^1H$  and  $L^2H$ ) electron from phenolic-OH will be more concentrated in the former. This destabilises the occupied molecular orbitals and stabilises the

unoccupied molecular orbitals for  $L^3H$ . Consequently the energy for electronic transition decreases and the band is red shifted to 353 nm. Additionally  $L^3H$  displays an additional shoulder at

**Table 7**  
pK<sub>a</sub> values for the ligands.

Ligands	pK <sub>1</sub>	pK <sub>2</sub>
L <sup>1</sup> H	4.1	10.7
L <sup>2</sup> H	4.1	10.0
L <sup>3</sup> H	4.2	10.6

408 nm which undergoes small blue shifting to 402 nm in complex **3**. Since this shoulder is only observed in **3**, it may involve electronic transition from occupied MO majorly contributed by naphthyl ring which is destabilised to small extent upon coordination to metal.

In the visible region the complexes **1** and **2** show two distinct bands in the region 490–500 nm and 712–716 nm. According to the literature for the tetracoordinated Cu complex [25] the former band may be assigned to a phenolate-to-Cu(II) charge transfer (LMCT) while the low energy peak is due to a d–d transition. However complex **3** exhibits a shoulder at 492 nm due to the phenolate-to-Cu(II) transition and has the d–d band at 620 nm (Fig. 6). Naphthyl group in L<sup>3</sup>H might have a dominant effect on the

electronic properties of complex **3**. The d–d band in complex **3** has been blue shifted by ~100 nm in comparison to complexes **1** and **2**. Since the d–d band results from transition between molecular orbitals with significant metal character, transition energy may be higher if the metal based occupied molecular orbitals get stabilized. In case of complex **3**, the Cu dominated occupied molecular orbitals may be more stabilized because of delocalization of the metal electron into the naphthyl ring. This kind of delocalization is restricted in the benzene ring of phenol moiety for complexes **1** and **2**.

### 3.4. EPR spectra

Cu<sup>II</sup> is EPR active. X-band EPR spectra of the complexes **1**, **2** and **3** in DMF at liquid nitrogen temperature are shown in Fig. 7. Analysis of the observed spectra indicates a typical Cu<sup>II</sup> complex with  $d_{x^2-y^2}$  or  $d_{z^2}$  ground state ( $S = 1/2$ ). All the spectra shows hyperfine and superhyperfine characteristics resulting from the interaction of unpaired electron of Cu<sup>II</sup> with nuclear spin of Cu [ $^{63,65}\text{Cu}$  ( $I = 3/2$ )] and the nitrogen ( $^{14}\text{N}$ ;  $I = 1$ ), respectively. In addition complex **3** displays the superhyperfine feature due to

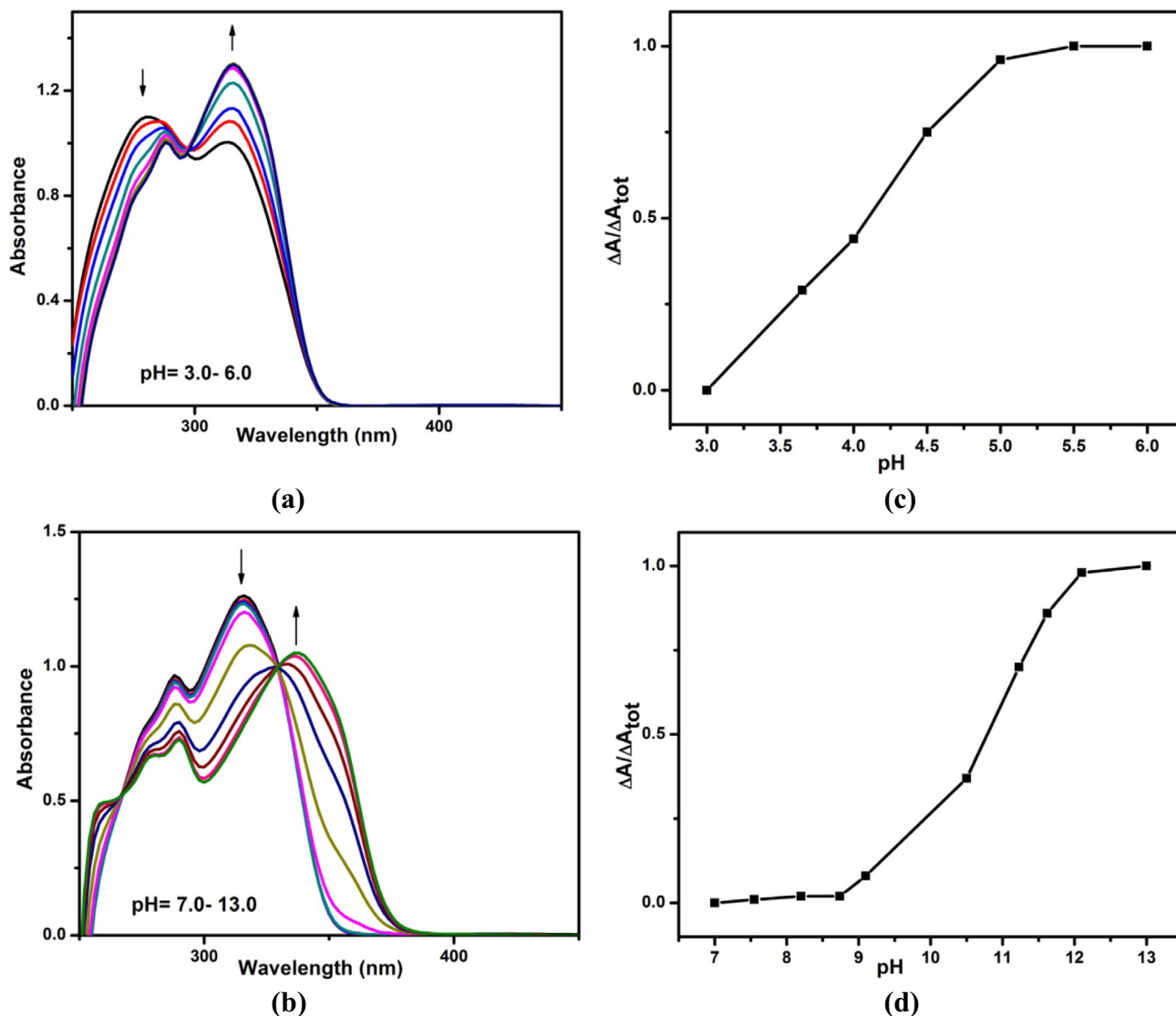


**Fig. 10.** Change in the absorption spectra of L<sup>1</sup>H in **a** (3–6 pH) and **b** (7–13 pH) with variation of pH in DMF–aqueous buffer (Robinson–Britton) solution (1:1). **c** and **d** represent the graphical method of L<sup>1</sup>H at 314 nm (3–6 pH) and at 336 nm (7–13 pH), respectively, change of  $\Delta A/\Delta A_{\text{tot}}$  vs. pH.

interaction of unpaired electron of  $\text{Cu}^{\text{II}}$  with nuclear spin of two coordinated imidazole nitrogen ( $^{14}\text{N}$ ;  $I = 1$ ) atoms. The spectral parameters are summarized in the Table 5.

### 3.5. TD-DFT calculation

TD-DFT calculation was performed on  $\text{L}^2\text{H}$  and corresponding complex **2** to explain the experimental absorption spectra. Vertical excitations with band position, oscillator strength and character assignment of the transition have been summarized in Table 6. The simulated UV–Vis spectral bands are in good resemblance with that of the experimental one for both the ligand and the complex. In DMF medium all the high energy UV region transition are ligand based and involves the participation of three rings: Phenol, imidazole and benzene. Ligand  $\text{L}^2\text{H}$  shows two peaks at 298 nm and 332 nm. Theoretically obtained band positions are 308 nm and 335 nm. The first transition ( $\lambda = 308$  nm) takes place from the imidazole ring to the phenyl ring at the 4 and 5 positions of the imidazole ring ( $\text{HOMO} \rightarrow \text{LUMO} + 1$ ), whereas the second transition ( $\lambda = 335$  nm) is from the imidazole ring to the phenol ring ( $\text{HOMO} \rightarrow \text{LUMO}$ ) (Fig. 8).

The complex has four bands in the UV region (296 nm, 335 nm, 344 nm, and 374sh nm) and two bands in the visible region (500 nm and 712 nm). The calculated transition in the UV region (293 nm, 335 nm, 350 nm and 367 nm) matches nicely with the experimental, whereas in the visible region (499 nm, 529 nm, and 666 nm) it deviates little bit.

In complex **2**, the transition at 293 nm ( $\lambda_{\text{exp}} = 296$  nm) is ligand centered  $\pi \rightarrow \pi^*$  transition ( $\text{HOMO} - 2(\text{A}) \rightarrow \text{LUMO}(\text{A})$  (36%)) from phenol to the phenol as well as imidazole ring with certain percentage to the benzene ring. 335 nm peak ( $\lambda_{\text{exp}} = 335$  nm) is dominated by the  $\pi \rightarrow \pi^*$  transition  $\text{HOMO} - 1(\text{A}) \rightarrow \text{LUMO} + 1(\text{A})$  (48%) in phenol rings. The peaks at 350 nm ( $\lambda_{\text{exp}} = 344$  nm) and 367 nm ( $\lambda_{\text{exp}} = 374$  nm) is also the transition between phenol rings. The transitions, respectively, are  $\text{HOMO}(\text{A}) \rightarrow \text{LUMO} + 1(\text{A})$  (21%) and  $\text{HOMO}(\text{A}) \rightarrow \text{LUMO}(\text{A})$  (17%). In experimental absorption spectra two peaks are obtained at 500 nm and 720 nm. In the simulated spectra we obtain two peaks at 499 nm ( $\text{HOMO} - 3(\text{B}) \rightarrow \text{LUMO}(\text{B})$  (33%)) and 529 nm ( $\text{HOMO} - 2(\text{B}) \rightarrow \text{LUMO}(\text{B})$  (29%)) corresponding to the experimental peak at 500 nm, both of which are phenolate to  $\text{Cu}^{\text{II}}$  transition. The lowest energy transition is obtained at 665 nm ( $\lambda_{\text{exp}} = 712$  nm), which is a d–d transition along with significant contribution from phenol/imidazole to  $\text{Cu}$  LMCT (Fig. 9).

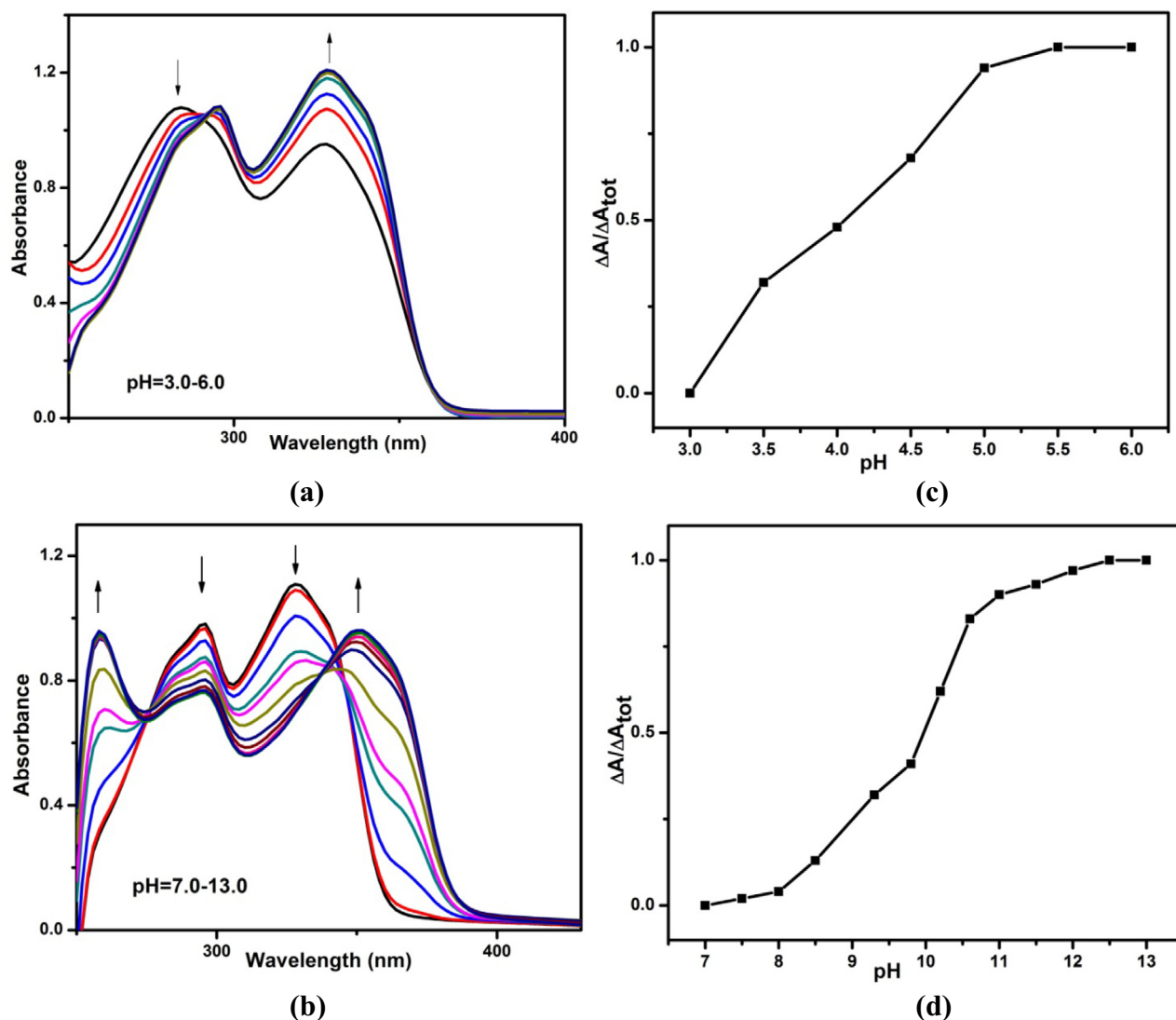
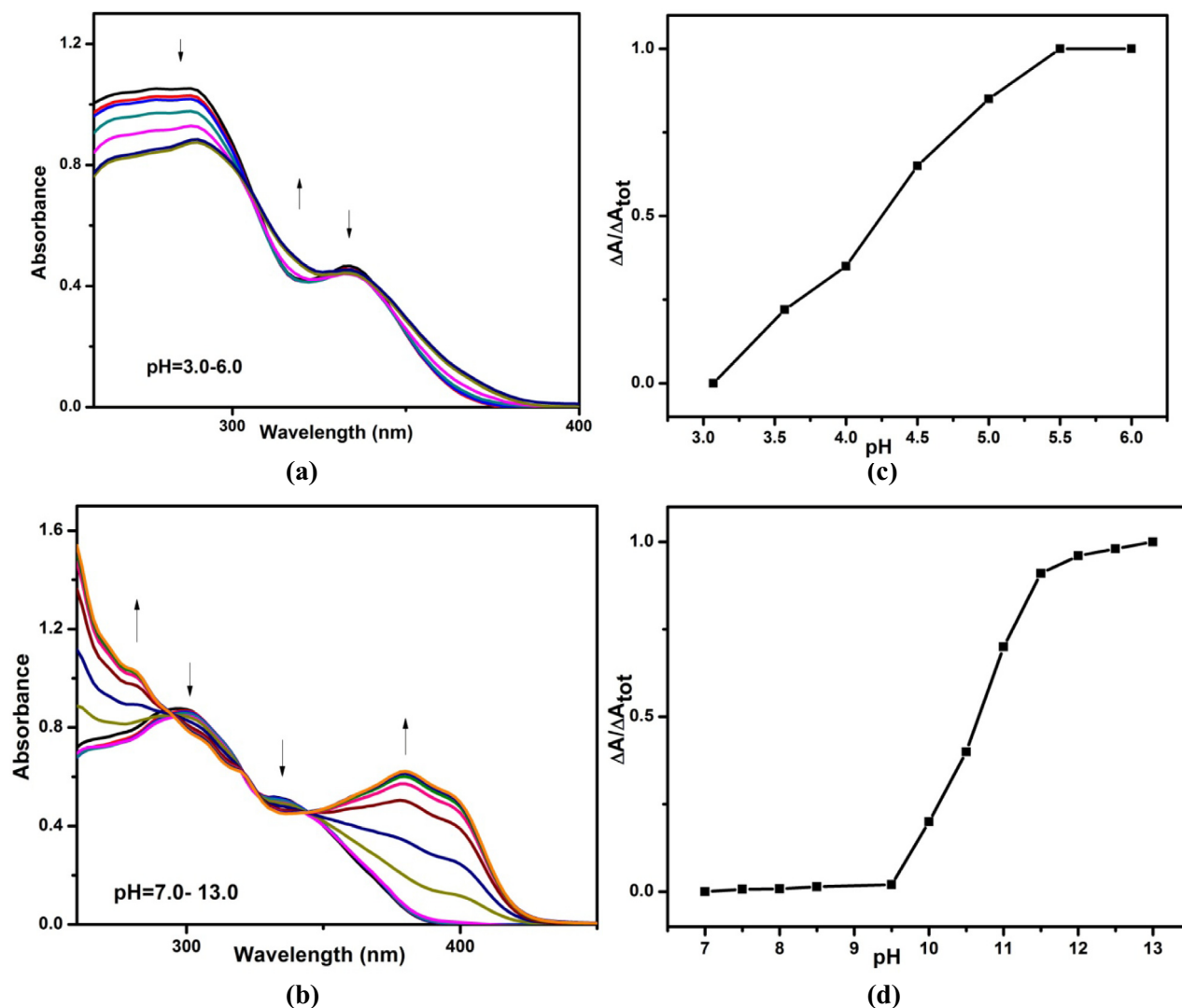
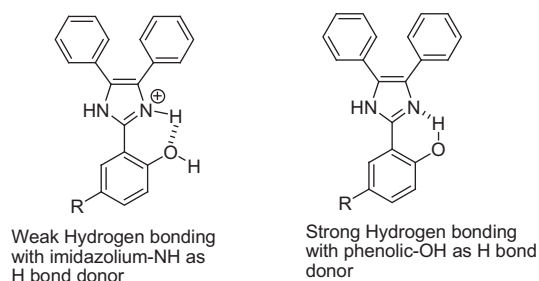


Fig. 11. Change in the absorption spectra of  $\text{L}^2\text{H}$  in a (3–6 pH) and b (7–13 pH) with variation of pH in DMF–aqueous buffer (Robinson–Britton) solution (1:1). c and d represent the graphical method of  $\text{L}^2\text{H}$  at 328 nm (3–6 pH) and at 350 nm (7–13 pH), respectively, change of  $\Delta A/\Delta A_{\text{tot}}$  vs. pH.



**Fig. 12.** Change in the absorption spectra of  $L^3H$  in **a** (3–6 pH) and **b** (7–13 pH) with variation of pH in DMF–aqueous buffer (Robinson–Britton) solution (1:1). **c** and **d** represent the graphical method of  $L^3H$  at 288 nm (3–6 pH) and at 380 nm (7–13 pH), respectively, change of  $\Delta A/\Delta A_{tot}$  vs. pH.



**Scheme 1.** Hydrogen bonding in phenol–imidazolium cation and phenol imidazole.

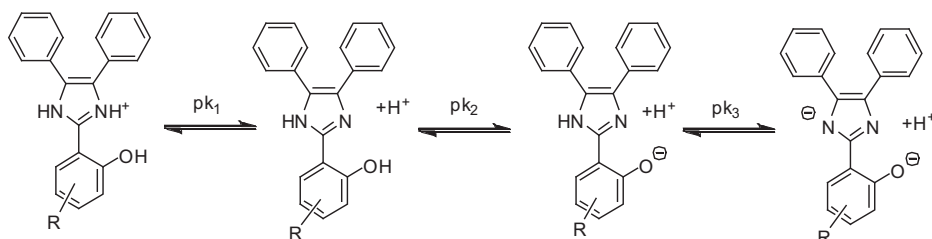
### 3.6. UV–Vis spectrophotometric titration and determination of $pK_a$

The influence of pH on the absorption spectral behavior of the ligands and complexes has been studied in DMF–aqueous buffer (Robinson–Britton) solution (1:1) over the pH range 3–13. The change in absorption spectra with varying pH is same for all the ligands and the complexes. From the inspection of two different range of pH, (3–6 and 7–13) two different deprotonation steps are observed.  $pK_a$  values were obtained by plotting absorbance parameters versus pH.  $pK_a$  values are given in Table 7. In the most

acidic pH the ligands are characterized by the peak at  $\sim 280$  nm, which is red shifted by 10 nm on changing the solution to neutral pH. At pH 7 the ligands  $L^1H$ ,  $L^2H$  and  $L^3H$  show a transition at 315 nm, 328 nm and 335 nm (shoulder), which undergo a bathochromic shift by 20 nm, 20 nm and 40 nm for  $L^1H$ ,  $L^2H$  and  $L^3H$ , respectively. In each case the absorption spectra shows isobestic point indicating the presence of interconverting species due to change in pH.

The absorbance changes ( $\Delta A$ ) are normalized by dividing by the total absorbance changes ( $\Delta A_{tot}$ ). The  $pK_a$  is taken as the pH at which  $\Delta A/\Delta A_{tot} = 0.5$  [26]. Graphically the  $pK_1$  is  $\sim 4.1$  and for  $pK_2$  is 10–10.7 due to the deprotonation of imidazolium-H and phenolic-OH, respectively. Assignments of the transitions have also been manifested by TD-DFT study on one of the representative ligand  $L^2H$ .

**$L^1H$ :** Between pH 3–6 the spectrum passes through one isobestic point at 296 nm. The peak at 278 nm (pH 3) is red shifted to 287 nm with a gradual decrease in absorbance whereas the intensity of the peak at 314 nm continuously increases. This corresponds to the imidazolium-H deprotonation,  $pK_1 = 4.1$ . At pH 7 the spectra corresponds to a phenol with a strong absorption band at 315 nm. On increasing the pH from 7 to 13 the spectrum passes through one isobestic point at 330 nm, a huge red shifting of the



Where R= H( $L^1H$ ), Br( $L^2H$ ), fused benzene ring ( $L^3H$ )

**Scheme 2.** Successive deprotonation of the imidazolium cation ( $pK_1$ ), phenol ( $pK_2$ ) and imidazole proton ( $pK_3$ ).

peak from 315 nm to 336 nm takes place. Intensity of the peak at 315 nm gradually decreases with a resultant increase in the 336 nm peak. This corresponds to the deprotonation of the phenolic-OH to form the corresponding phenoxide,  $pK_2 = 10.7$ . UV-Vis spectral titration and the plot for  $pK_a$  is displayed in Fig. 10.

**$L^2H$ :** UV-Vis spectral titration and the plot for  $pK_a$  for  $L^2H$  is displayed in Fig. 11. At pH 3, where the species is exclusively in the imidazolium form, there are two bands at 284 and 328 nm. On changing the pH from 3 to 6 the spectrum passes through one isobestic point at 290 nm. The peak at 284 nm (pH 3) is red shifted to 295 nm with a gradual decrease in absorbance whereas the intensity of the peak at 328 nm continuously increases. This corresponds to the imidazolium-H deprotonation,  $pK_1 = 4.1$ . At neutral pH (7) the phenolic form exist and the species is characterized by two sharp bands at 295 nm and 328 nm. In the range of pH 7–13 the spectrum passes through two isobestic points at 274 nm and 336 nm, with the following observation: a new peak is developed at 258 nm, decrease in intensity of the 295 nm peak and red shifting of the 328 nm peak to 350 nm. This corresponds to the deprotonation of the phenolic-OH,  $pK_2 = 10.0$ .

**$L^3H$ :** Between pH 3–6, the spectrum passes through three isobestic points at 305 nm, 327 nm and 342 nm. On changing the pH from 3 to 6, a nominal red shifting of 1 nm takes place for the broad peak at 288 nm with gradual decrease in intensity. A very little decrease in intensity also takes place for the peak at 334 nm. This corresponds to the imidazolium-H deprotonation,  $pK_1 = 4.2$ . In the range of pH 7–13 the spectrum passes through three isobestic points 293 nm at 322 nm and 345 nm. Characteristic peaks of 300 nm and 335 nm shoulder at pH 7, completely vanishes with the development of a new peak at 380 nm and a shoulder at 398 nm on reaching to pH 13. This corresponds to the deprotonation of the phenolic-OH,  $pK_2 = 10.6$ . UV-Vis spectral titration and the plot for  $pK_a$  for  $L^3H$  is displayed in Fig. 12.

$pK_a$  for the deprotonation of the imidazolium ion is 7.0. In the present system this process occurs with  $pK_a \sim 4.1$ . This enhanced acidity may be due to the extra stability of the conjugate base achieved via the hydrogen bond formed between the phenolic-OH (H-bond donor) and the imidazole-N (H-bond acceptor). In the imidazolium form this hydrogen bond is not favorable as both the N atoms of the imidazole ring remain protonated and imidazole/imidazolium N cannot act as H-bond acceptor. There is a possibility of weak H-bonding when imidazolium/imidazole NH acts as H-bond donor and phenolic-O as electron acceptor (Scheme 1).

In all the ligands  $pK_a$  for the phenolic-OH is greater than phenol (9.95), since phenolic-OH is expected to remain hydrogen bonded to the imidazole-N intramolecularly. The trend in  $pK_2$  may be explained on the basis of the substitution in the phenol ring. Br ( $L^2H$ : 10.0) has the maximum -I effect leading to highest acidity followed by fused benzene ring ( $L^3H$ : 10.6) and H ( $L^1H$ : 10.7). However, in the conjugate base, the (-)ve charge on the phenoxide ion may also get stabilized through delocalization into the benzene or naphthyl ring of the phenol. Simultaneously there is a possibility

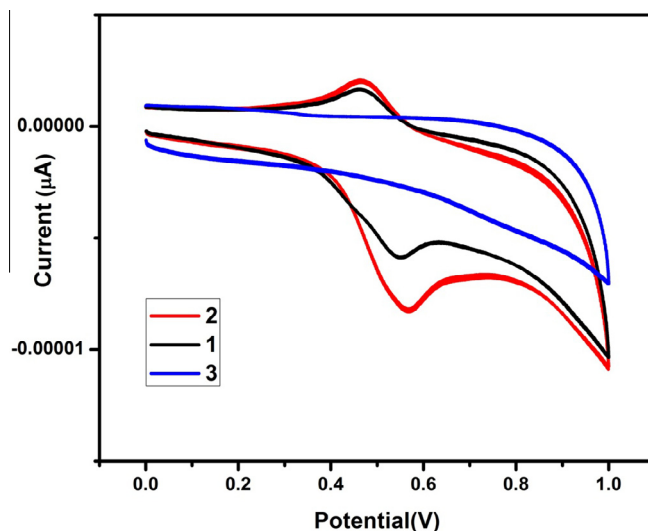


**Fig. 13.** Cyclic voltammograms of **1**, **2** and **3** in DMF:H<sub>2</sub>O (8:2) solution with TEAP in glassy carbon electrode at 100 mV/s.

**Table 8**  
Cyclic voltammetric data for  $L^1H$ ,  $L^2H$ ,  $L^3H$ , **1**, **2** and **3**.

Lig/complex	E <sub>pa</sub> (V)	E <sub>pc</sub> (V)	E <sub>1/2</sub> (V)	ΔE (mv)
$L^1H$	0.563	0.474	0.51	89
$L^2H$	0.857	0.759	0.80	98
$L^3H$	0.435	0.362	0.39	73
<b>1</b>	0.553	0.459	0.50	94
<b>2</b>	0.566	0.465	0.51	101
<b>3</b>	...	...	...	...

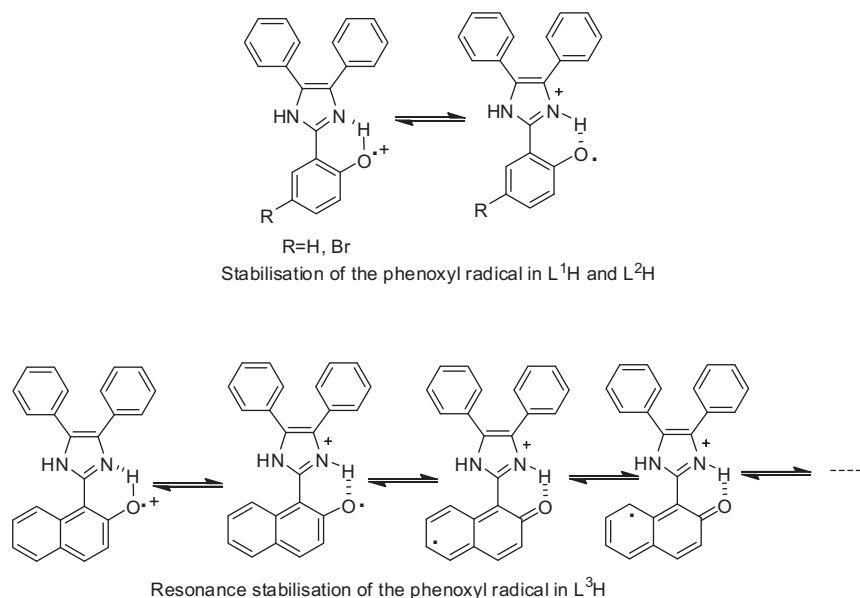
of hydrogen bond between the phenoxide-O and the imidazole-NH, the later comes close to the former by the rotation of the C-C bond connecting the phenol and imidazole ring.

So the observed trend may a combination of these two effects in the conjugate base of the phenol. However due to the precipitation at pH >13, the  $pK_a$  for the imidazole-H ( $pK_3$  in the Scheme 2) could not be determined.

On the basis of the observed data following deprotonation process may be proposed.

### 3.7. Redox properties

The electrochemical behavior of the phenolic ligands and their Cu complexes were studied by cyclic voltammetry. Cyclic voltammetry in DMF:H<sub>2</sub>O (8:2) solution of all the ligands show a quasi-reversible-reversible peak in the anodic scan in the range 0.435–0.857 V. This peak is due to oxidation of phenol to phenoxyl radical



**Scheme 3.** Stabilisation of phenoxyl radical via hydrogen bonding (L<sup>1</sup>H, L<sup>2</sup>H) and hydrogen bonding and resonance (L<sup>3</sup>H).

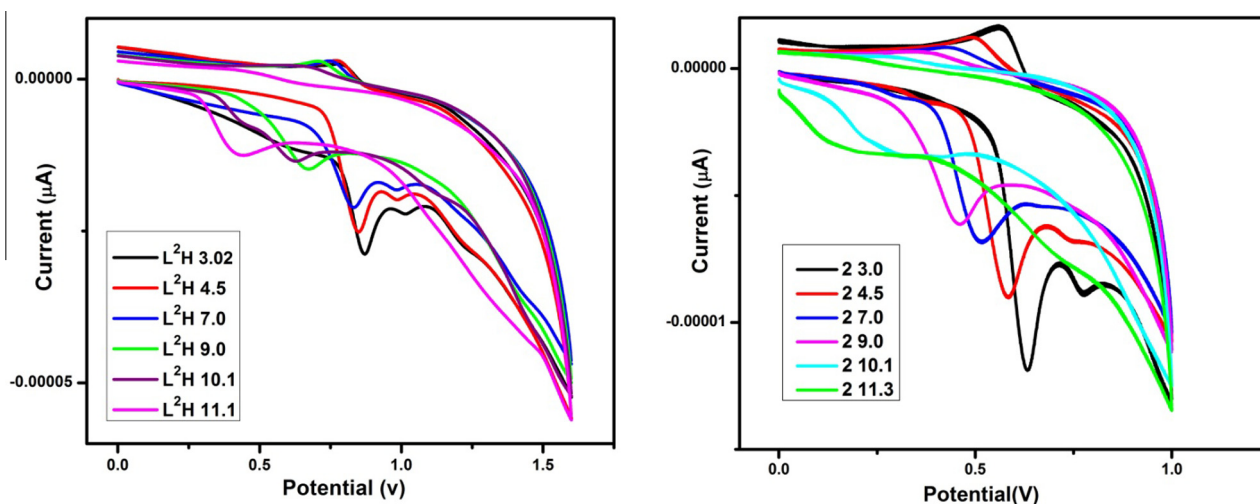


**Fig. 14.** Cyclic voltammograms of L<sup>2</sup>H and complex 2 at variable pH (3–11) recorded in DMF:H<sub>2</sub>O (8:2) solution with TEAP supporting electrolyte in glassy carbon electrode at scan rate 100 mV/s.

[13–16]. For complexes 1 and 2 the potential are 0.553 V and 0.566 V respectively, whereas complex 3 does not display any oxidation on anodic scan (Fig. 13). The cyclic voltammetric data are given in the Table 8. The pH of the solution (DMF:H<sub>2</sub>O (8:2)) of the complexes used in this study are in the range 8–8.5. During the pH dependent study we noted that, this is the terminal pH value, above which the oxidation peak is not resolved clearly. For complex 3, at high pH (>8) the negative charge of phenoxide ion may enter into naphthalene ring in addition to the delocalisation to the metal orbitals and is unavailable for the oxidation. For all the complexes this reasoning is applicable. But due to fused ring, naphthalene ring can snatch the phenoxide (complex 3) electron density to larger extent than phenol ring (complexes 1 and 2). Consequently complex 3 with pH=8.5 (pH of the solution (DMF:H<sub>2</sub>O (8:2)) used in Cyclic voltammetry) does not display any phenolic-OH-phenoxyl radical oxidation. According to the earlier reports [5,14] these types of mixed imidazole-phenol ligands undergo proton assisted electron transfer. The  $E_{ox}^0$  for the phenol

to phenoxyl radical conversion is much less than usual value of 1.01 V. This extra stability of the phenoxyl radical is facilitated by hydrogen bonding. When there is an intramolecular proton acceptor near to the phenolic-OH, H atom of phenoxyl radical may be attached to the base leading to a H-bonded resonance stabilised structure [10,17]. In our case the imidazole-N acts as a proton acceptor and the oxidized form remains as depicted in Scheme 3. The lowest  $E^0$  value for L<sup>3</sup>H may be due to the delocalisation of the phenoxyl radical electron inside the naphthyl ring, leading to large number of resonance stabilised forms.

Potential of this oxidation wave changes with pH. On increasing pH from 3 to 11 the  $E^0$  gradually reduces. In most acidic medium (at pH = 3) the  $E^0$  is in the range 0.86–0.50 which reduces by 0.22 V in the most alkaline pH. Cyclic voltammogram of ligand L<sup>2</sup>H and complex 2 is given in Fig. 14. The pK<sub>a</sub> for the phenolic functionality obtained in our system falls in the region 10.0–10.7. Deprotonation of phenolic-OH starts after pH 8.5. So the oxidation becomes more easy when phenol is present as phenoxide anion.

The oxidized phenoxyl radical formed in this case may also get stabilised by H-bonding between the phenoxyl-O and the imidazole-N. At same pH the ligand based oxidation in the Cu complexes take place at a lower potential. This may be due to the metal assisted stability of the phenoxyl radical in the complex. With varying pH a similar trend in  $E^0$  for the metal complex as that of the ligand is also observed. In the complex **3**, the oxidation peak is not observed at higher pH. At pH >8.5 the solution in the cyclic voltammetry cell turned turbid.

#### 4. Conclusion

The phenol–imidazole ligand reported in this work is a redox non-innocent system. Its electrochemical property is highly pH dependent as evident from the cyclic voltammogram at variable pH. The ligands contain three sites that can show acid–base equilibrium, namely imidazolium-N, Phenolic-OH and imidazole N-H.  $pK_a$  of imidazolium N (~4.1) is much less than the imidazole (7) itself due to the stability for the conjugate base through hydrogen bonding. But  $pK_a$  for the phenolic-OH moiety is slightly higher than phenol itself (9.95) as the conjugate base does not get extra stability by some means, e.g., hydrogen bonding like the first dissociation process. Phenol-phenoxyl oxidation process is much easier than the phenol itself. Presence of an imidazole base at the ortho position stabilizes the oxidized product through intramolecular hydrogen bonding. With respect to the ligands the Cu complexes show similar to lower  $E^0$  values for the phenol/phenoxyl radical oxidation process. The lower  $E^0$  value may be due to the metal based stability of the phenoxyl radical. The potential of the ligands as well as for the complex is close to the naturally occurring Galactose Oxidase. So these types of molecules may be screened as catalyst for alcohol oxidation.

#### Acknowledgments

S.N. thanks CSIR, New Delhi, Govt. of India for funding this work through CSIR Project (No. 01(2577)/12/EMR-II, 03/04/2013). S.N. is grateful to AICTE, New Delhi, Govt. of India for sanctioning a UV–Vis–NIR spectrophotometer through AICTE-RPS Project (No. 8023/RID/RPS-10/Pvt (II Policy)/2011–12). The authors thank CIF, BIT–Mesra, Ranchi, India for analytical measurements. A.P. thanks UGC, New Delhi, India for MANF–JRF fellowship.

#### Appendix A. Supplementary data

CCDC 1057462 contains the supplementary crystallographic data for **2.DMF**. These data can be obtained free of charge via <http://www.ccdc.cam.ac.uk/conts/retrieving.html>, or from the Cambridge Crystallographic Data Centre, 12 Union Road,

Cambridge CB2 1EZ, UK; fax: (+44) 1223-336-033; or e-mail: [deposit@ccdc.cam.ac.uk](mailto:deposit@ccdc.cam.ac.uk).

Supplementary data associated with this article can be found, in the online version, at <http://dx.doi.org/10.1016/j.poly.2015.06.014>.

#### References

- [1] J. Stubbe, W.A. Van der Donk, *Chem. Rev.* 98 (1998) 705.
- [2] J.W. Whittaker, *Chem. Rev.* 103 (2003) 2347.
- [3] J. Stubbe, D.G. Nocera, C.S. Yee, M.C.Y. Chang, *Chem. Rev.* 103 (2003) 2167.
- [4] I. Vass, S. Styring, *Biochemistry* 30 (1991) 830.
- [5] C. Costentin, M. Robert, J.M. Savéant, *Phys. Chem., Chem. Phys.* 12 (2010) 11179.
- [6] C. Costentin, C. Louault, M. Robert, J.M. Savéant, *Proc. Nat. Acad. Sci. U.S.A.* 106 (2009) 18143.
- [7] C. Costentin, C. Louault, M. Robert, J.M. Savéant, *J. Am. Chem. Soc.* 130 (2008) 15817.
- [8] I.J. Rhile, J.M. Mayer, *J. Am. Chem. Soc.* 126 (2004) 12718.
- [9] I.J. Rhile, T.F. Markle, H. Nagao, A.G. DiPasquale, O.P. Lam, M.A. Lockwood, K. Rotter, J.M. Mayer, *J. Am. Chem. Soc.* 128 (2006) 6075.
- [10] F. Thomas, O. Jarjayes, H. Jamet, S. Hamman, E. Saint-Aman, C. Duboc, J.L. Pierre, *Angew. Chem., Int. Ed.* 43 (2004) 594.
- [11] G.M. Zats, H. Arora, R. Lavi, D. Yufit, L. Benisvy, *Dalton Trans.* 41 (2012) 47.
- [12] G.M. Zats, H. Arora, R. Lavi, D. Yufit, L. Benisvy, *Dalton Trans.* 40 (2011) 10889.
- [13] L. Benisvy, A.J. Blake, D. Collison, E.S. Davies, C.D. Garner, E.J.L. McInnes, J. McMaster, G. Whittaker, C. Wilson, *Chem. Commun.* (2001) 1824.
- [14] L. Benisvy, A.J. Blake, D. Collison, E.S. Davies, C.D. Garner, E.J.L. McInnes, J. McMaster, G. Whittaker, C. Wilson, *Dalton Trans.* (2003) 1975.
- [15] L. Benisvy, E. Bill, A.J. Blake, D. Collison, E.S. Davies, C.D. Garner, C.I. Guindy, E.J.L. McInnes, G. McArdle, J. McMaster, C. Wilson, J. Wolowska, *Dalton Trans.* (2004) 3647.
- [16] L. Benisvy, E. Bill, A.J. Blake, D. Collison, E.S. Davies, C.D. Garner, G. McArdle, E.J.L. McInnes, J. McMaster, S.H.K. Ross, C. Wilson, *Dalton Trans.* (2006) 258.
- [17] L. Benisvy, R. Bittl, E. Bothe, C.D. Garner, J. McMaster, S. Ross, C. Teutloff, F. Neese, *Angew. Chem., Int. Ed.* 44 (2005) 5314.
- [18] A. Kochem, A. Carrillo, C. Philouze, M.V. Gastel, A. Hardemare, F. Thomas, *Eur. J. Inorg. Chem.* (2014) 4263.
- [19] D.T. Sawyer, A. Sobkowiak, J.L. Roberts Jr., *Electrochemistry for Chemists*, second ed., John Wiley and Sons, New York, 1995, p. 333.
- [20] G.M. Sheldrick, *SHELXS-97*, Program for Crystal Structure Solution, University of Göttingen, Göttingen, Germany, 1997.
- [21] G.M. Sheldrick, *SHELXL-97*, Program for the Refinement of Crystal Structures from Diffraction Data, University of Göttingen, Göttingen, Germany, 1997.
- [22] L.J. Farrugia, *J. Appl. Crystallogr.* 32 (1999) 837.
- [23] M.J. Frisch, G.W. Trucks, H.B. Schlegel, G.E. Scuseria, M.A. Robb, J.R. Cheeseman, J.A. Montgomery, T. Vreven Jr., K.N. Kudin, J.C. Burant, J.M. Millam, S.S. Iyengar, J. Tomasi, V. Barone, B. Mennucci, M. Cossi, G. Scalmani, N. Rega, G.A. Petersson, H. Nakatsuji, M. Hada, M. Ehara, K. Toyota, R. Fukuda, J. Hasegawa, M. Ishida, T. Nakajima, Y. Honda, O. Kitao, H. Nakai, M. Klene, X. Li, J.E. Knox, H.P. Hratchian, J.B. Cross, C. Adamo, J. Jaramillo, R. Gomperts, R.E. Stratmann, O. Yazyev, A.J. Austin, R. Cammi, C. Pomelli, J.W. Ochterski, P.Y. Ayala, K. Morokuma, G.A. Voth, P. Salvador, J.J. Dannenberg, V.G. Zakrzewski, S. Dapprich, A.D. Daniels, M.C. Strain, O. Farkas, D.K. Malick, A.D. Rabuck, K. Raghavachari, J.B. Foresman, J.V. Ortiz, Q. Cui, A.G. Baboul, S. Clifford, J. Cioslowski, B.B. Stefanov, G. Liu, A. Liashenko, P. Piskorz, I. Komaromi, R.L. Martin, D.J. Fox, T. Keith, M.A. Al-Laham, C.Y. Peng, A. Nanayakkara, M. Challacombe, P.M.W. Gill, B. Johnson, W. Chen, M.W. Wong, C. Gonzalez, J.A. Pople, *Gaussian 09*, Gaussian, Inc., Wallingford, CT, 2004.
- [24] L. Yang, D.R. Powell, R.P. Houser, *Dalton Trans.* (2007) 955.
- [25] R.H. Holm, G.W. Everett Jr., A. Chakravorty, *Inorg. Chem.* 7 (1966) 83.
- [26] C.R. Johnson, R.E. Shepherd, *Inorg. Chem.* 22 (1983) 1117.